A proteomic view of cellular responses of macrophages to copper when added as ion or as copper-polyacrylate complex

Bastien Dalzon, Julie Devcic, Joanna Bons, Anaëlle Torres, Hélène Diemer, Stéphane Ravanel, Véronique Collin-Faure, Sarah Cianférani, Christine Carapito, Thierry Rabilloud

This document is an author version of a paper published in Journal of Proteomics (2021) under the doi: 10.1016/j.jprot.2021.104178

A proteomic view of cellular responses of macrophages to copper when added as ion or as copper-polyacrylate complex

Bastien Dalzon[1], Julie Devcic[1], Joanna Bons [2], Anaelle Torres[1], Hélène Diemer [2], Stéphane Ravanel[3,] Véronique Collin-Faure[1], Sarah Cianferani[2], Christine Carapito[2], Thierry Rabilloud[1] *

1-Chemistry and Biology of Metals, Univ. Grenoble Alpes, CNRS UMR5249, CEA, IRIG-LCBM, F-38054 Grenoble, France

2-Laboratoire de Spectrométrie de Masse BioOrganique (LSMBO), Université de Strasbourg, CNRS, IPHC UMR 7178, 67000 Strasbourg, France

3-Univ. Grenoble Alpes, INRAE, CNRS UMR5168, CEA-IRIG, LPCV, Grenoble, F-38000 France

*: to whom correspondence should be sent

Abstract

Copper is an essential metal for life, but is toxic at high concentrations. In mammalian cells, two copper transporters are known, CTR1 and CTR2. In order to gain insights on the possible influence of the import pathway on cellular responses to copper, two copper challenges were compared: one with copper ion, which is likely to use preferentially CTR1, and one with a copper-polyacrylate complex, which will be internalized via the endosomal pathway and is likely to use preferentially CTR2. A model system consisting in the J774A1 mouse macrophage system, with a strong endosomal/lysosomal pathway, was used. In order to gain wide insights into the cellular responses to copper, a proteomic approach was used. The proteomic results were validated by targeted experiments, and showed differential effects of the import mode on cellular physiology parameters.
While the mitochondrial transmembrane potential was kept constant, a depletion in the free glutahione content was observed with copper (ion and polylacrylate complex). Both copper-polyacrylate and polyacrylate induced perturbations in the cytoskeleton and in phagocytosis. Inflammatory responses were also differently altered by copper ion and copper-polyacrylate. Copper-polyacrylate also perturbed several metabolic enzymes. Lastly, enzymes were used as a test set to assess the predictive value of proteomics.

Significance:
Proteomic profiling provides an in-depth analysis of the alterations induced on cells by copper under two different exposure modes to this metal, namely as the free ion or as a complex with polyacrylate. The cellular responses were substantially different between the two exposure modes, although some cellular effects are shared, such as the depletion in free glutathione. Targeted experiments were used to confirm the proteomic results. Some metabolic enzymes

showed altered activities after exposure to the copper-polyacrylate complex. The basal inflammatory responses were different for copper ion and for the copper-polyacrylate complex, while the two forms of copper inhibited lipopolysaccharide-induced inflammatory responses

1. Introduction

As for several metallic elements such as zinc or iron, copper is essential for life but becomes toxic at high concentrations. For example, a defect in copper excretion is the cause of the hereditary Wilson and Menkes diseases [1]. The toxic properties of copper led to its widespread usage as a biocide, e.g. in agriculture as a fungicide (see [2] for a review), with consequences on human health among workers (e.g. in[3]). More recently and in a more subtle way, copper has been promoted for anticancer strategies, e.g. in [4–6] . These strategies rely on copper ionophores to increase the intracellular copper concentrations to reach cytotoxicity in target cells at copper concentrations that are not systemically toxic. Using ionophores is indeed a way to circumvent the deactivation of the copper membrane transporter CTR1 by endocytosis upon copper excess conditions [7].
Several mechanisms have been proposed to explain the toxicity of the copper complexes, including proteasome inhibition [4,8] or oxidative stress [9,10]**.** The two mechanisms may be linked, as copper induces oxidative alteration of the proteasome and thus its inhibition [11].
It is clear that the therapeutic effect is due to an increase in the intracellular copper concentration [12]. However, it seems that a higher sensitivity of cancer cells to proteasome inhibition [13] or oxidative stress compared to normal cells [14,15] is more likely to explain this effect than a differential increase in copper concentration between normal and cancer cells [16].
This leads to a potential way of improving the contrast in toxicity between normal and cancer cells, or toward suppressor myeloid cells that are interesting targets in anticancer approaches [17,18]. As a first approach in this direction, we decided to test two different entry routes for copper ion in cells, either classically through the plasma membrane as free ion, or through the endocytic pathway via a complex of copper ion with an anionic polymer, in our case polyacrylate, as polymeric polyanions are well known to be unable to cross the plasma membrane. This route was intended to use the lysosomal pathway for copper entry [19], and may rely upon the alternate copper transporter CTR2 [20], which is localized in endosomes and lysosomes [21].

In order to get a better appraisal of the cellular responses to these treatments, we decided to use a proteomic approach, which gives a substantially wider view of the cellular reactions to toxicants than targeted approaches (see for example [22–24] for reviews), and validated the most striking results of the proteomic screen by targeted experiments.

2. Materials and methods

Unless specified otherwise, the chemicals used in this work were purchased from Sigma-Millipore and were at least 99% pure. As a copper source for the copper complexes, we used a titrated copper sulfate solution (4% catalog number C2284). Sodium polyacrylate (average molecular mass 15,000, #416037) was purchased directly as a water solution and sterilized by pasteurization at 80°C overnight.

2.1. Cell culture

The mouse monocyte/macrophage cell line J774A1 was purchased from the European Cell Culture Collection (Salisbury, UK). The cells were cultured in DMEM + 10% fetal bovine serum. Cells were seeded every two days at 200,000 cells/ml and harvested at 1,000,000 cells per ml. For treatment with chemicals, the following scheme was used: cells were first seeded at 500,000 cells/ml in T175 flasks (50 ml per flask). They were exposed to copper ion (150µM), polyacrylate (0.25 mg/ml final concentration) or a combination of both on the following day and harvested after a further 4 hours or 24 hours in culture. Cell viability was measured by the neutral red uptake assay [25]. All experiments were carried out at least in triplicate on independent cultures.

2.2. Subcellular fractionation and ion quantification by ICP-MS

For measuring copper uptake in cells and its repartition, the cells were harvested after exposure to copper ion, polyacrylate or polyacrylate + copper ion by scraping in buffer A (Hepes 10 mM pH 7.5, sucrose 200 mM, magnesium chloride 2 mM), and collected by centrifugation (500 g, 5 min).
In some experiments the cell pellet (ca 50µl in volume) was resuspended in 500 µl of buffer A to which 0.15 % (w/v) tetradecyldimethylammonio propane sulfonate (SB 3-14) was added. After lysis for 20 minutes on ice, the protein concentration was determined by a modified dye-binding assay [26] and the lysate was stored frozen at -20°C until mineralization.
In other experiments, the cell pellet was resuspended in 500 µl of buffer A on ice, and the cells were lysed in a Dounce homogeneizer by ten strokes of the tight pestle. The homogenate was first centrifuged at 1000g for 5 minutes at +4°C to remove unbroken cells and nuclei. The supernatant was collected and centrifuged at 15000g for 20 minutes at +4°C. The supernatant was collected and saved, and the pellet (particulate fraction) was resuspended in 500µl of buffer A. The protein concentration of both extracts (particulate and supernatant) was determined by a modified dye-binding assay [26].

The extracts were then mineralized by the addition of one volume of suprapure 65% HNO_3 per volume of extract and incubation on a rotating wheel at room temperature for 18 h.

Mineralized samples were diluted in distilled water and analyzed using an iCAP RQ quadrupole mass instrument (Thermo Fisher Scientific GmbH, Germany) equipped with an ASX-560 auto-sampler (Teledyne CETAC Technologies, Omaha, USA). The instrument was used with a MicroMist U-Series glass concentric nebulizer, a quartz spray chamber cooled at 3°C, a Qnova quartz torch, a nickel sample cone, and a nickel skimmer cone equipped with a high-sensitivity insert. Elements were analyzed using kinetic energy discrimination mode with helium as the collision cell gas (for ^{63}Cu and ^{65}Cu). Concentrations were determined using standard curves and corrected using an internal standard solution of 103Rh added online. Data integration was done using the Qtegra software (version 2.8.2944.115). The background equivalent concentration (BEC) on pure standards was 0.02 ng/ml for ^{63}Cu and ^{65}Cu.

2.3. Proteomics

For this study, 2D gel-based proteomics was used. After cell treatment with copper ion, polyacrylate, or their combination for 24 hours, as described above, the culture medium was removed and the cells collected by scraping in Hepes saline (Hepes 10mM pH 7.5, NaCl 150mM and MgCl2 2mM). After two rinses in the same solution, the cell pellet was lysed by the addition of ten cell pellet volumes of lysing solution (urea 7M, thiourea 2M, CHAPS 4%, TCEP-HCl 5mM, spermine base 15mM, spermine tetrahydrochloride 15mM). After 30

minutes at room temperature to complete cell lysis, the lysate was centrifuged (16,000g, 30 minutes, room temperature) to pellet the nucleic acids. The protein-containing supernatant was collected and the protein concentration determined by a modified dye binding assay [26]. Carrier ampholytes (0.4% final concentration) were then added and the lysates were stored frozen at -20°C until use.
2D gel-based proteomics was carried out as previously described [27], using linear pH 4-8 gradients in the focusing dimension, 10% polyacrylamide gels in the second dimension and silver staining. The gels were scanned after silver staining on a flatbed scanner (Epson perfection V750), using a 16 bits grayscale image acquisition. The gel images were then analyzed using the Delta 2D software (v 4.7). Spot identification was carried out by nanoLC-MS/MS analysis on a nanoACQUITY Ultra-Performance-LC (Waters Corporation, Milford, MA, USA) coupled to a TripleTOF 5600 instrument run in Data Dependent Acquisition mode (Sciex,Framingham, MS, USA) as previously described [27]. The mass spectrometry data are deposited in PRIDE [28] under the accession number PXD021252.

For statistical analyses, the difference between two groups was determined by a Student T-test or a Mann Whitney U-test. For the global analysis of the spot abundances data, we used directly the spot abundances data as provided by the gel analysis software. The software directly normalizes each spot abundance by the sum of all spot abundances detected on the gel. These relative abundances data were used directly for global analysis using the PAST software suite [29] without any transformation. Hierarchical clustering was selected as the analysis method for its insensitivity to missing or null values. In order to minimize the quantitative bias due to different protein abundances, the Gower distance (i.e. a normalized distance) was used to perform the clustering analysis.

2.4. Enzyme assays

The enzymes were assayed according to published procedures (see below).

The cell extracts for enzyme assays were prepared by lysing the cells for 20 minutes at 0°C in Hepes 20 mM pH 7.5, $MgCl_2$ 2 mM, KCl 50 mM, EGTA 1 mM, tetradecyldimethylammonio propane sulfonate (SB 3-14) 0.15 % (w/v), followed by centrifugation at 15,000 g for 15 minutes to clear the extract. The protein concentration was determined by a dye-binding assay [26].

The dehydrogenases or dehydrogenases-coupled activities were assayed at 500nm using the phenazine methosulfate/iodonitrotetrazolium coupled assay [30]. The enzyme assay buffer contained Hepes NaOH 25mM pH 7.5, magnesium acetate 5mM, potassium nitrate 100mM and Triton X-100 (1% w/v). It also contained 30µM phenazine methosulfate, 200µM iodonitrotetrazolium chloride, 250µM of the adequate cofactor (NAD or NADP) and 1-5mM of the organic substrate, which was used to start the reaction. For phosphate-dependent enzymes such as glyceraldehyde dehydrogenase (GAPDH) and purine phosphorylase (PNPH), 50mM potassium phosphate pH 7.5 was added to the enzyme assay buffer. Transaldolase was assayed by a GAPDH coupled assay [31].

Purine phosphorylase (PNPH) was assayed by a xanthine oxidase--coupled assay [32]. Enolase was assayed at 340nm by a pyruvate kinase-lactate dehydrogenase-coupled assay [33]. Aspartate aminotransferase was assayed by a glutamate dehydrogenase-coupled assay [34]. Lactoylglutathione lyase activity was assayed at 240 nm as previously described [35].

2.5. In gel detection of malate dehydrogenase activity

The enzyme was detected by a phenazine methosulfate/nitrobuetetrazolium assay after in-gel renaturation [36]. Briefly, 0.5 mg of protein extract was loaded on a 2D gel and separated as described previously. Immediately after electrophoresis, an 8x5 cm gel piece was cut in the region containing malate dehydrogenase, as determined from previous proteomic experiments providing x-y coordinates for the malate dehydrogenase spots on the 2D gels. The excised zone was chosen to leave room for eventual modified or cleaved malate dehydrogenase forms. The proteins were renatured by immersing the gel piece for 2x20 minutes in a solution containing TrisHCl buffer pH 7.5 50mM, NaCl 200mM, Glycerol 10% (v/v) Triton X-100 2% (w/v) and DTT 1mM, under reciprocal shaking. The gel piece was then further renatured by a 2x20 minutes treatment by the same solution without DTT. Finally, the activity was detected by immersing the gel piece in a solution containing Tris buffer pH 7.5 80mM, NaCl 10mM, MgCl2 5mM, disodium malate 50mM, phenazine methosulfate 2.5 µg/ml, NAD 1mg/ml and nitro tetrazolium blue 2.5 mg/ml. The activity was detected by blue spots on a transparent background. Finally, the gel piece, was rinsed several times with water, scanned to produce a digital image as described above, and counterstained with colloidal Coomassie blue. Major spots detected by Coomassie Blue in the excised region were used as anchor spots to carry the excised zone on the general 2D spot pattern.

2.6. Phagocytosis assay

The phagocytic activity was measured using fluorescent latex beads (1 µm diameter, green labelled, catalog number L4655 from Sigma), as described previously [37,38]. After a 2h30 treatment with the fluorescent beads in culture medium at 37°C, the cells were harvested in PBS). Phagocytic activity was measured by flow cytometry on a FacsCalibur instrument (Beckton Dickinson).

2.7. F-Actin staining

The experiments were performed essentially as previously described [39]. The cells were cultured on coverslips placed in 6-well plates, and exposed to copper ion, polyacrylate or both, as described above. At the end of the exposure time, cells were washed twice for 5 min at 4°C in PBS, fixed in 4% paraformaldehyde for 30 min at room temperature. After two washes (5 min/4°C in PBS), they were permeabilized in Triton X100 (0.1% w/v) for 5 min at room temperature. After two more washes in PBS, Phalloidin-Atto 550 (Sigma) (500 nM) was added to the cells and let for 20 min at room temperature in the dark. Coverslips-attached cells were washed, placed on microscope slides (Thermo Scientific) using a Vectashield mounting medium containing DAPI (Eurobio) and imaged using a Zeiss LSM 800 confocal microscope. The images were processed using the ImageJ software.

2.8. Mitochondrial transmembrane potential measurement

The mitochondrial transmembrane potential was assessed by Rhodamine 123 uptake [40], using a low Rhodamine concentration (80 nM) to avoid intramitochondrial fluorescence quenching that would result in a poor estimation of the mitochondrial potential [41]. The samples were analyzed by flow cytometry on a FacsCalibur instrument (Beckton Dickinson). Both the proportion of rhodamine positive cells and the mean fluorescence of this population were recorded in the analysis.

2.9. Glutathione assay

Cellular reduced glutathione was assayed by an in vivo conjugation assay [27] based on the conjugation of glutathione to chlorodinitrobenzene by the cellular glutathione S-transferases [42].

2.10. NO and cytokines production

The cells were grown to confluence in a 6 well plate and pre-treated with copper ion, polyacrylate or both, as described above. For the final 18 hours of culture, half of the wells were treated with 100 ng/ml LPS (from salmonella, purchased from Sigma), and arginine monohydrochloride was added to all the wells (5 mM final concentration) to secure a high concentration of substrate for the nitric oxide synthase. After 18 hours of incubation, the cell culture medium was recovered, centrifuged at 10,000 g for 10 minutes to remove cells and debris. The supernatants were used for nitrite determination by the Griess reagent [27] and for cytokine measurements using a cytokine bead assay (BD Cytometric Bead Array, catalog number 552364 from BD Biosciences).

3. Results and Discussion

3.1. Cellular copper uptake and content

Previous experiments have shown that copper ion in the 100-200 μM range was sufficient to induce functional effects on macrophages after a 24 hours exposure [38]. We thus started by fixing a 150 μM concentration for the copper ion concentration. We then determined the polyacrylate concentration that, in combination with 150 μM copper ion, induced a cellular mortality of less than 20% after a 24 hours exposure, leading to the 0.25mg/ml value used. This concentration was added as polyacrylate alone as a further control condition. The rationale for using polyacrylate as a copper carrier was that polyacrylate is known to bind to the scavenger receptor [43], and is thus targeted to the endosomal/lysosomal pathway, where the CTR2 copper transporter is located [20,21]. Conversely, free copper ion is supposed to be transported by the plasma membrane transporter CTR1[44], although the divalent metal transporter DMT1 can also play a role [45].

We first checked if this exposure led to an increase in the intracellular copper concentration, and to which extent. Thus, in a first series of experiments, the copper concentration of the total cell lysate was determined by ICP-MS after a 24 hours exposure to copper ion, polyacrylate and copper-polyacrylate. The background value was 16±15 ng/mg cellular protein (untreated cells) while cells treated with polyacrylate alone showed a copper content of 6±1 ng/mg cellular protein (not significantly different, $p=0.43$). Cells treated with 150μM copper ion showed a copper content of 8370±1750 ng/mg cellular protein, while cells treated with copper ion and polyacrylate showed a copper content of 6900±1780 ng/mg cellular protein. The two latter values were not significantly different ($p=0.36$) while the two values obtained for copper treated cells were significantly different from those obtained for cells untreated with copper ($p<0.025$). The fact that the copper ion and copper-polyacrylate treatments induced a similar total intracellular copper content suggests that possible differential effects should not be linked to the total intracellular copper concentration by itself, but rather to the differences in the entry pathways and thus in the subcellular distribution of copper.

In order to gain further insight in the difference of copper uptake pathway, which was expected in our experimental scheme, the cellular copper content was determined after 4 hours of exposure both in the particulate fraction, containing the mitochondria, the endosomes and the peroxisomes, and in the supernatant fraction. This time frame was selected to be short enough to avoid complete intracellular equilibration, which could take place in a 24 hours exposure, but long enough to allow sufficient and measurable copper accumulation. The results, displayed in **Table 1** (with the original data in **Suppl. Table 1**), showed that in unexposed conditions, the majority of the cellular copper was found in the particulate fraction. However, when cells were exposed to excess copper, the majority of the cellular copper was found in the supernatant fraction. This may be due to metallothionein induction by copper, although the selected copper concentration may be borderline to induce metallothioneins [46], but also to the fact that many cellular proteins are able to bind copper when present in excess [47,48].

Table 1 : copper ion concentration in cellular fractions

condition	Cu particulate (P)	Cu supernatant (S)	Cu (P+S)
control	42.5±10.8	23.6±11	27.8±10.6
polyacrylate	41.5±3.9	15.1±2.5	19.9±2.3
Cu ion	465.7±73.1*	2657±312*	2355±283*
Cu-polyacrylate	759±76.7*†	2376±219*	2156±204*

Copper concentrations are expressed in ng copper/mg cellular proteins.
Protein concentrations in the particulate fractions were 0.35±0.1 mg/ml, and 1.87±0.28 in the supernatant fraction, and were not significantly different between the copper-treated and non-treated samples (see supplementary Table 1 for details)
* : significantly different from control ($p<0.01$)
† : significantly different from copper ion ($p<0.01$)

Moreover, while there was no significant difference in the total copper concentration between the samples treated with copper ion and those treated with the copper-polyacrylate complex, the particulate fraction of the copper-polyacrylate complex-treated samples contained significantly more copper than the particulate fraction of the copper ion-treated samples ($p<0.01$). No significant difference could be observed between the control and polyacrylate-treated samples. These results on short exposure experiments support our initial hypothesis that copper ion and copper-polyacrylate complex do not use the same pathways to enter the cells.

3.2. Global analysis of the proteomic results

Representative 2D gel images are shown on **Figure 1**, and all the raw images used for this project are available in **Suppl Figs 1-4**. 2442 spots were detected and quantified on the gels (**Suppl Table 2**), of which 164 were significantly altered ($p<0.05$) by at least one of the treatments and unambiguously identified by mass spectrometry (**Suppl. Table 3**). The

identification parameters are given in **Suppl Table 4**. As another statistics-based selection, a Mann Whitney U-test was performed and the proteins showing a U value of 0 (i.e. unidirectional p-Value of 0.05) were selected (**Suppl Table 5**). These selection criteria meant in turn that for a protein appearing as multiple spots, a significant change for one spot was considered as significant for the protein, as a modified form may have a strongly modified activity (increased or decreased) compared to the main spot owing to classical post-translational modifications such as phosphorylation (e.g.in [49]) or acylation [50] or to oxidation through an oxidative stress mechanism (e.g. in [51]).

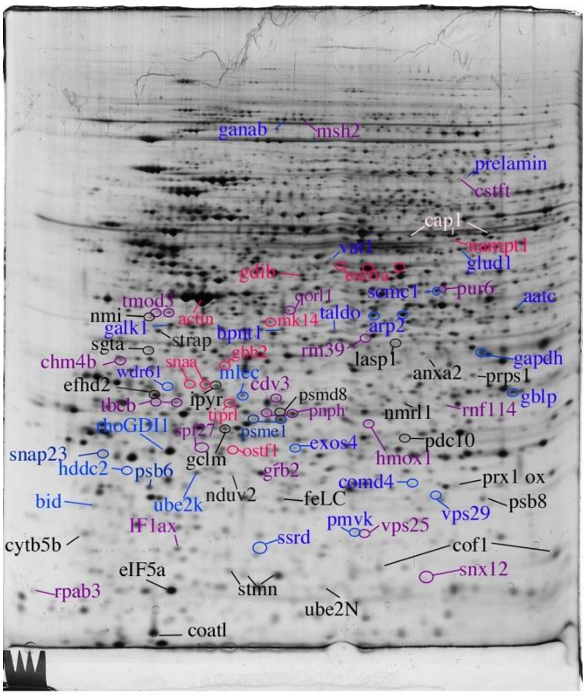
ganab
msh2
prelamin
cstft
cap1
nampt1
vat1
glud1
gdib
scmc1
pur6
aatc
tmod3
gorl1
nmi
actin
mk14
taldo
galk1
bpnt1
arp2
sgta
strap
rm39
lasp1
gapdh
chm4b
snaa
gbb2
wdr61
mlec
cdv3
efhd2
anxa2
prps1
ipyr
gblp
tbcb
psmd8
pnph
nmrl1
rnf114
rhoGDI1
spf27
psme1
exos4
hmox1
pdc10
snap23
gclm
ostf1
hddc2
psb6
grb2
comd4
prx1 ox
bid
ube2k
nduv2
feLC
vps29
psb8
IF1ax
pmvk
vps25
cytb5b
ssrd
cof1
eIF5a
snx12
rpab3
stmn
ube2N
coatl

A

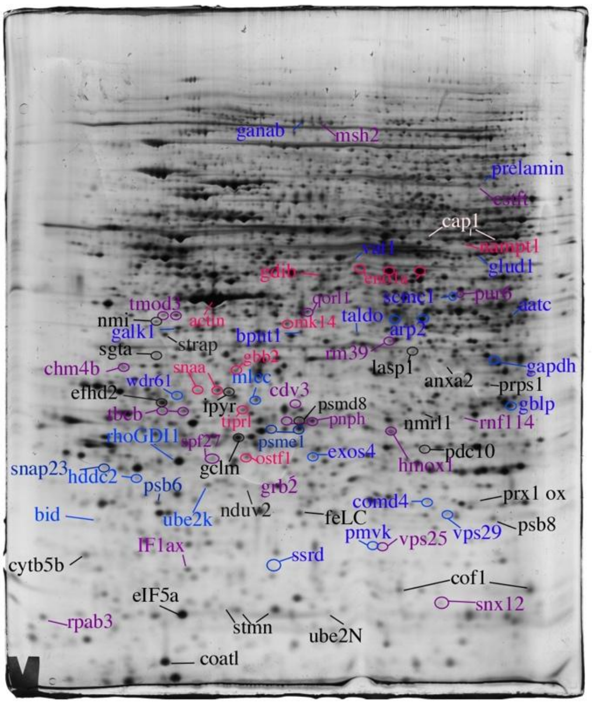

B

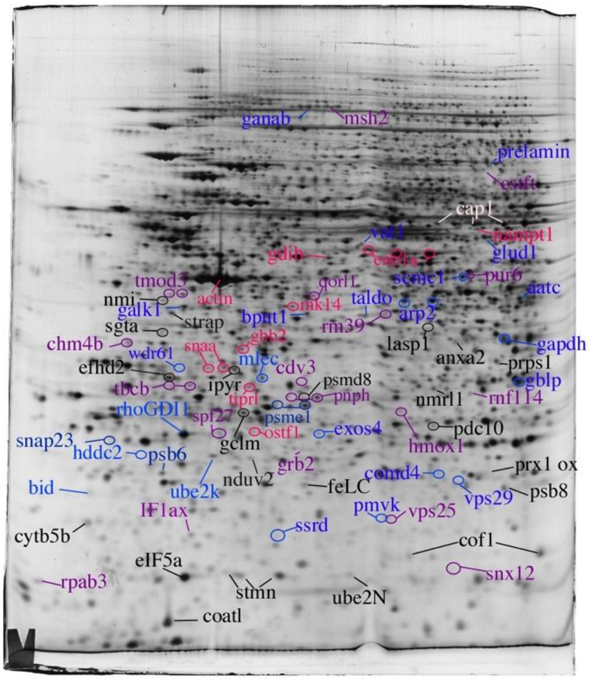

C

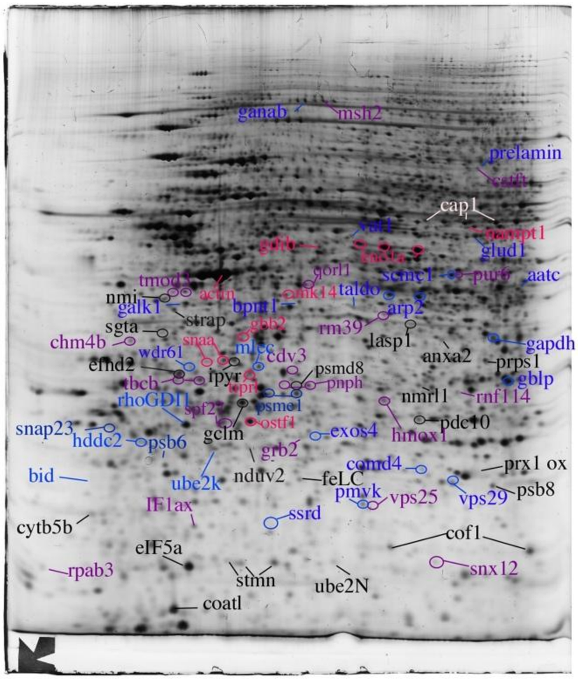

D

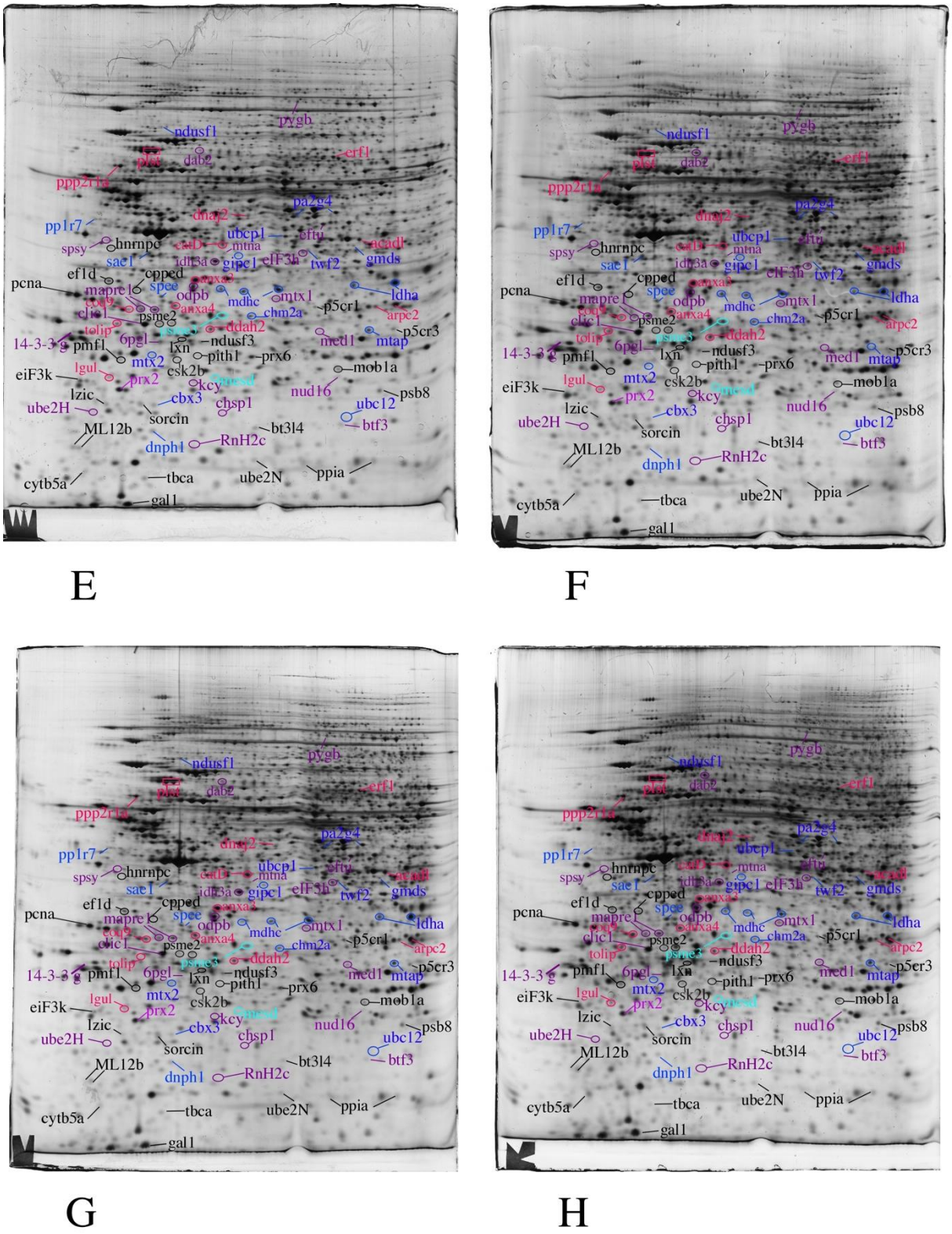

Figure 1 : Proteomic analysis of total cell extracts by 2D electrophoresis
Total cell extracts of RAW274.7 cells were separated by two-dimensional gel electrophoresis. The first dimensions covered a 4-8 pH range and the second dimension a 15-200 kDa range. Total cellular proteins (150 µg) were loaded on the first dimension gel.

A,E: gel obtained from unexposed cells
B,F: gel obtained from cells exposed to 150 µM copper sulfate
C,G: gel obtained from cells exposed to 0.25 mg/ml polyacrylate

D,H: gel obtained from cells exposed to 0.25 mg/ml polyacrylate + 150µM copper sulfate

The colors in the web version of the figure have been chosen only for legibility purposes.

As the treatments used (i.e. copper ion, polyacrylate or their combination) are not independent, but linked together, we used the proteomic data to perform a hierarchical clustering analysis, in order to determine how the effects of the different treatments applied on cells ranked compared to the control situation. Hierarchical clustering has the advantage to be insensitive to null or missing values, thereby requiring no data imputation, and is generally easy to interpret. These features explain why it has been one of the first methods used to globally analyze proteomic results [52–54], and is still used to sort the relative impact of various conditions in a multi conditions experimental scheme (e.g. in [27,55–57].
The results are shown on **Figure 2**. The biological replicates for each condition were grouped together, and the clustering pattern indicated that the two treatments containing polyacrylate (i.e. polyacrylate alone and copper+polyacrylate) were more different from the control than the treatment with copper ion alone. Although counterintuitive in the frame of effects mainly driven by copper, this result represents the overall outcome of the proteomic experiments. When interpreting this result, it should be kept in mind that this analysis takes into account all the 2442 spots. Thus, coordinated changes, which appear as not significant when taken individually, are very likely to impact the clustering. Thus, this method may prove sensitive to weak but coordinated changes that escape the classical, statistics-based, protein selection used in most of the proteomic experiments.

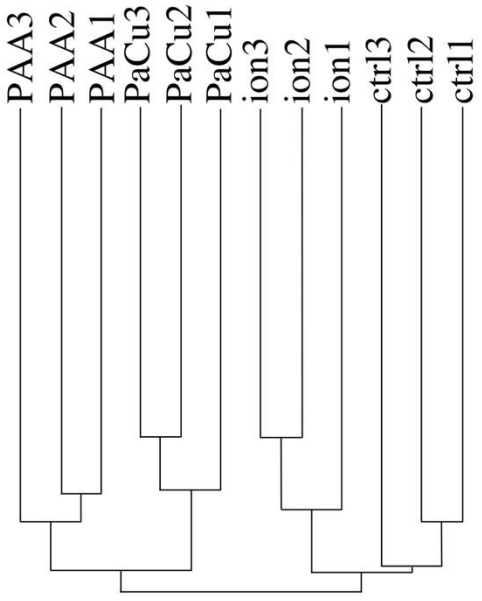

Figure 2: Global analysis of the proteomic experiment by hierarchical clustering

Quantitative proteomic data (i.e. spots intensities in 2D gel-based proteomics) were used to determine the similarities between biological samples. The PAST software package was used for the calculations, using the Gower similarity index and a Paired group algorithm. This tree indicates the similarity between the various experimental groups (the higher the distance of the branching point between groups, the more dissimilar they are).

Ctrl(1-3) : unexposed cells
ion(1-3) : cells exposed to 150 µM copper sulfate

PAA(1-3) : cells exposed to 0.25 mg/ml polyacrylate
PaCu (1-3): cells exposed to 0.25 mg/ml polyacrylate + 150µM copper sulfate

Biologically speaking, this result suggests that polyacrylate alone has a significant impact on macrophages. In this respect, the situation is clearly different from the one observed with the hydroxyquinoline-copper complex, where hydroxyquinoline alone showed a weak impact on the proteome [27].

3.3. The ubiquitine proteasome pathway is altered by copper treatment

As a first screen of the proteomic results, pathway analyses were carried out for each treatment using the DAVID tool [58] (**Suppl Tables 6-8**). In the case of copper ion, pathway analysis highlighted the proteasome **(Suppl Table 6)**. This pathway was also detected for the copper-polyacrylate complex treatment **(Suppl Table 8)**, which was biologically consistent.

3.4 Central metabolism enzyme activities are altered by copper and/or polyacrylate treatments

One other major pathway that was altered is "carbon metabolism", which appeared in all conditions (**Suppl Tables 6-8**). Enzymes belonging to the major classes of the central metabolism were found modulated such as enzymes of the pentose phosphate pathway, glycolysis, and amino acid metabolism. This prompted us to further test some of these enzymes in targeted experiments, and the results are displayed in **Table 2**.

Table 2: Enzyme activities

Enzyme †	control	Copper ion	Polyacrylate	Polyacrylate+Cu
AATC	3.92±0.58	4.08±0.95	4.33±0.63	5.33±0.63*§
enolase	281±13	257±5§	213±21*§	131±7**§
GAPDH	94 .2±7.1	94.5±8.2	88.9±4.3	78.2±3.5*§
LDH	108±1	110±9	104±8	97±11§
LGUL	27.9±1.7	30.3±1.1	35.9±2.7*§	31.7±1.8§
MDH	41.8±2.8	37.7±1.6	37.3±0.8§	31.7±2.0*§
PNPH	15.8±2.2	23.4±2*§	12.5±2	13.7±4.5
TALDO	20.4±0.5	21.1±0.6	23.1±1.1*§	20.1±1.1

† enzymes full names :
aatc : aspartate aminotransferase ; GAPDH : glyceraldehyde phosphate dehydrogenase ; LDH : lactate dehydrogenase ; LGUL : lactoylglutathione lyase ; MDH : malate dehydrogenase ; PNPH : purine nucleotide phosphorylase ; TALDO : transaldolase ;
All activities are expressed in nmole substrate converted/min/mg total protein.
* $p<0.05$ in the treated vs control comparison (Student T test)
** $p<0.01$ in the treated vs control comparison (Student T test)
§ $p<0.05$ in the treated vs control comparison (Mann Whitney U test)

One activity (enolase) was changed by all treatments. Copper ion modulated a second activity (purine phosphorylase). In addition to enolase, polyacrylate modulated another three enzyme activities (lactoylglutathione lyase, malate dehydrogenase and transaldolase). Besides enolase, copper-polyacrylate modulated another five activities, of which two ((lactoylglutathione lyase

and malate dehydrogenase) were also modulated by polyacrylate. Three additional activities (aspartate aminotransferase, glyceraldehyde phosphate dehydrogenase and lactate dehydrogenase) were modulated only by the copper-polyacrylate complex. Thus overall, copper-polyacrylate was the treatment with the most important impact on metabolic enzymes.

3.5. Use of enzyme activities to back-probe proteomic results

Proteomics and transcriptomics share the fact that they highlight differences based on amounts only. However, biology inference is made from amounts to function in most of the omics publications, either directly or indirectly through pathway analyses. This direct inference has been pointed as a potential issue [59], especially when confronted with the multiple layers of cellular regulations, as recently reviewed [60]. In this global frame, enzymes are one of the very few examples where the relevant biological outcome (i.e. the activity) can be relatively easily measured, allowing in turn to assess important features for the proteomic analyses, such as the positive predictive value (i.e. number of true positives /(number of true positives+number of false positives), or the sensitivity (number of true positives detected by proteomics/ total number of true positives). We thus compiled the statistical values for the proteomic experiments and the enzyme activity measurements in **Suppl Table 9**. Taking the assumption that a true positive is an enzyme activity change at $p \leq 0.05$, then the positive predictive value (PPV) of 2D gel proteomics at the $p \leq 0.05$ threshold is 50 % (7/14), with a sensitivity of 77 % (7/9). Although this PPV value is very close to the 40% PPV value that can be calculated from a shotgun proteomic experiment on mitochondria [61], these values should be not taken as generic, and may vary greatly from one proteomic experiment to another.

It may be argued that enzymes may be regulated differently from other cellular proteins. However, the scope of proteins identified in phosphoproteome [62] or acetylome [63] studies extends far beyond enzymes, so that assuming that enzymes are not regulated by different mechanisms than other proteins appears reasonable. This suggests that the statistical values obtained when comparing proteomic to activity results for enzymes may be extended globally to the complete proteomic experiment.

This question is further complicated in the case of 2D proteomics because many proteins, including enzymes, appear as multiple spots, and it is thus difficult to correlate a priori the biological activity with a subset of spots or the sum of all spots corresponding to the same protein. Beyond simple correlative approaches (e.g. in [40]) we were able to address this question for malate dehydrogenase, for which 2D zymography was successful. The results, shown in **Figure 3**, assigned the activity to the two most-basic spots identified on the 2D gels.

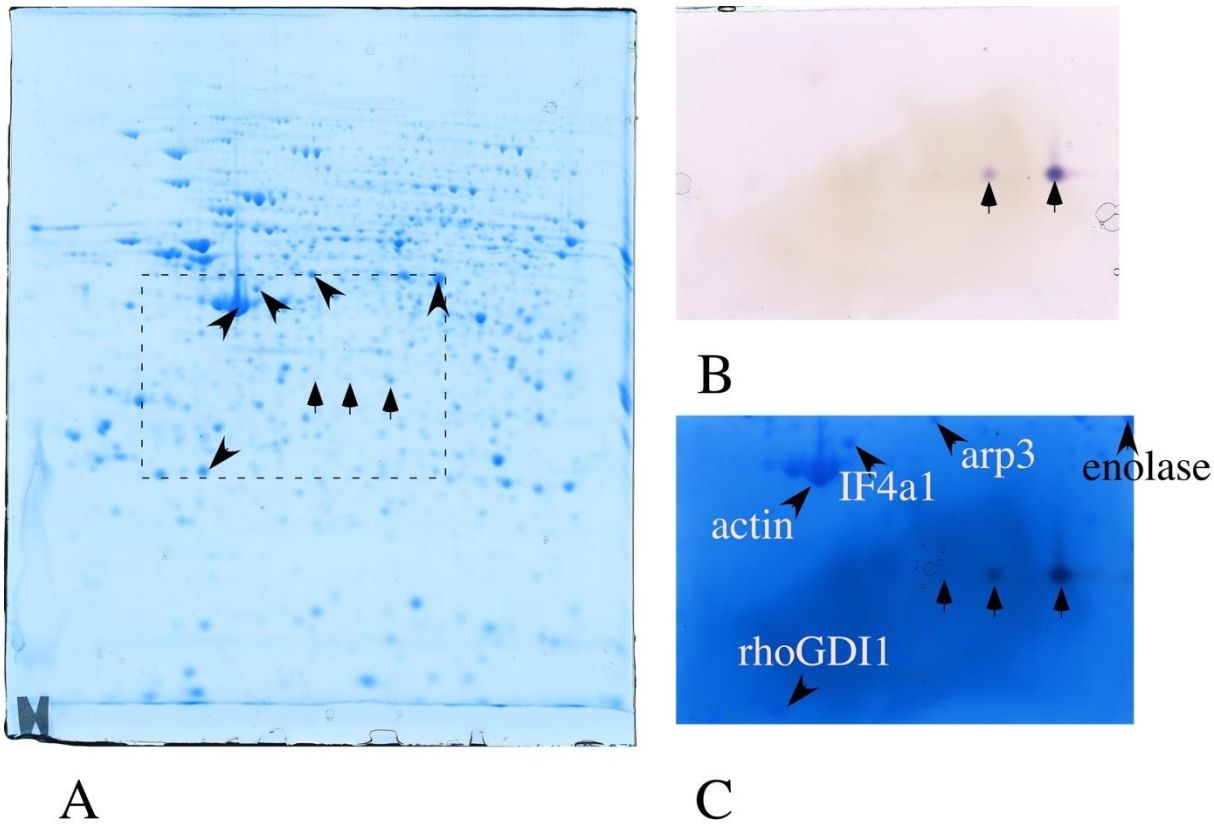

Figure 3: Assignment of active protein forms for malate dehydrogenase activity

500 µg of total cellular extract from control cells were loaded on two 2D gels run in parallel. One gel was directly stained by colloidal Coomassie blue (A). On the unstained second gel, a gel piece was cut according to the dashed rectangle drawn on the stained gel. The gel piece was then submitted to in gel renaturation and then detection of the malate dehydrogenase activity (B), and finally to counterstaining by colloidal Coomassie blue (C).
Vertical arrows: position of the malate dehydrogenase spots
arroweads : landmark proteins.

3.6. Mitochondrial function is maintained at non-toxic copper concentrations

The keyword « mitochondrion » also appeared in the pathway analysis **(Suppl Tables 6-8).** This is not surprising, as mitochondria are known to be an important actor in intracellular copper storage and homeostasis [64]. In this frame, the observed increase of the copper concentration in the particulate fraction (containing mitochondria) after a 4 hours exposure to copper ion (Table 1) strongly suggests an increase in intramitochondrial copper concentration, with potential deleterious effects. We thus investigated the global functioning of mitochondria by probing the transmembrane mitochondrial potential. The results, shown on **Figure 4,** indicated a small but significant ($p<0.01$) reduction in the proportion of rhodamine-positive cells upon treatment with copper-polyacrylate complex, suggesting a decreased viability induced by this treatment. This was in line with the known slight mortality induced by the copper-polyacrylate treatment.

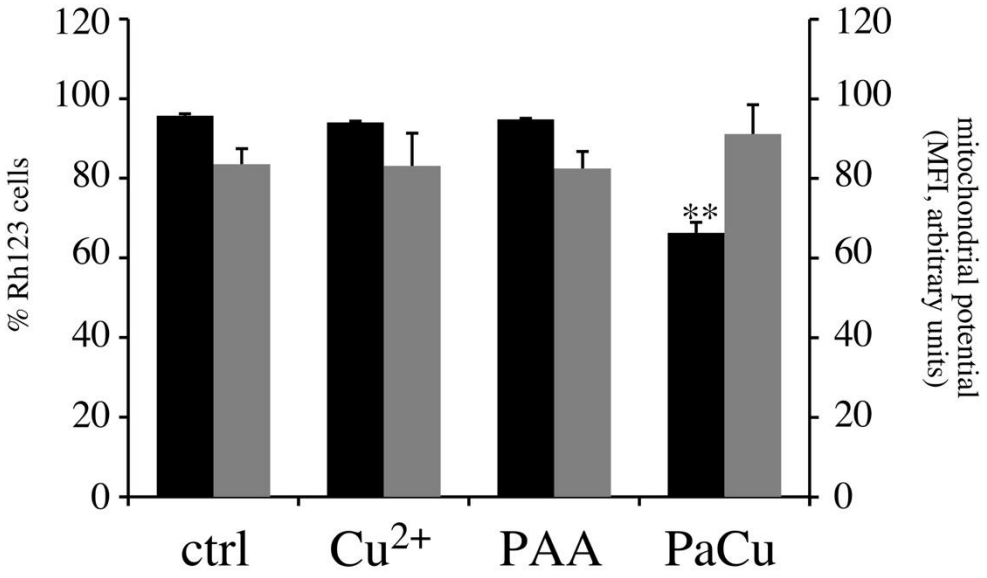

Figure 4 : Analysis of the mitochondrial transmembrane potential

The mitochondrial potential was analyzed by the rhodamine 123 accumulation method
black bars: proportion of positive cells in the viable cell population
grey bars: mean cellular fluorescence

Ctrl : unexposed cells
Cu^{2+} : cells exposed to 150 µM copper sulfate
PAA : cells exposed to 0.25 mg/ml polyacrylate
PaCu : cells exposed to 0.25 mg/ml polyacrylate + 150µM copper sulfate
Symbols indicate the statistical significance (Student T- test): *: $p<0.05$; **:$p<0.01$; ***: $p<0.001$

In addition, it should be noted that most of the significant changes in the amounts of mitochondrial proteins induced by the various treatments are increases. This strongly suggests that these increases are a compensatory mechanism set in place by the cells to maintain mitochondrial function in spite of the increased copper content, explaining the constant transmembrane mitochondrial potential that we observed. Interestingly, the type of effects (reduction in proportion of rhodamine-positive cells, no effect on the value of the transmembrane mitochondrial potential) were also observed with the hydroxyquinoline-copper complex [27].

3.7. The reduced glutathione level is decreased by copper

One of the proteins that was strongly induced after treatment with copper ion or copper-polacrylate complex was GCLM, i.e. the regulatory subunit of the enzyme involved in the first step of glutathione biosynthesis, which is the limiting step of the pathway [65]. We thus investigated the levels of free glutathione, as previous studies have shown a reduction in the levels of free glutathione upon treatment of macrophages with copper-quinoline complexes [27] or copper oxide nanoparticles [38]. The results, shown on **Figure 5,** indicated a significant reduction upon treatment with copper or copper complex, but not with polyacrylate alone, following the trend indicated by GCLM expression. Thus, copper in all its forms i.e. ionic, as a polyacrylate complex (this study), as a hydroxyquinoline complex [27] or as nanoparticles [38], induces a decrease in the cellular content of free glutathione.

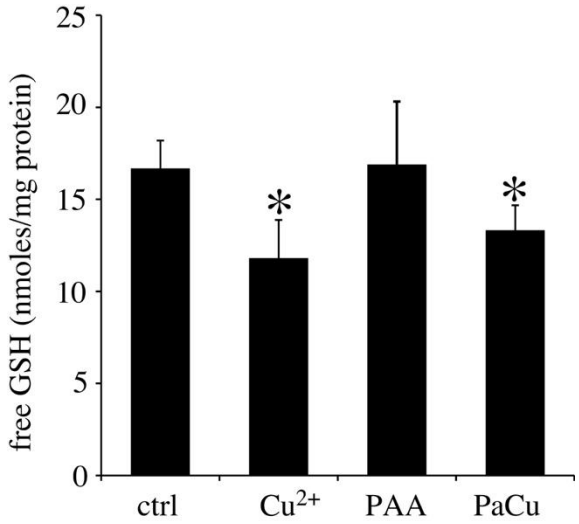

Figure 5 : glutathione levels
The glutathione level was measured by the CDNB conjugation method, and normalized to the protein content of the cells

Ctrl : unexposed cells
Cu^{2+} : cells exposed to 150 µM copper sulfate
PAA ; cells exposed to 0.25 mg/ml polyacrylate
PaCu : cells exposed to 0.25 mg/ml polyacrylate + 150µM copper sulfate
Symbols indicate the statistical significance (Student T- test): *: $p<0.05$; **:$p<0.01$; ***: $p<0.001$

3.8. The actin cytoskeleton and phagocytic activity are altered by treatment with polyacrylate and copper-polyacrylate

The proteomic screen **(Table 2)** and the pathway analysis pointed to actin cytoskeleton as one of the major modulated function upon copper treatment, for example through proteins involved in cell shape, adhesion and motility **(Suppl Tables 6&8)**. As a change in COATL detected by proteomics correlated with changes in the actin cytoskeleton [66], this prompted us to test how actin cytoskeleton responded to the treatments used in this study. The results, shown on **Figure 6 A-D**, indicated a minimal effect of copper ion on the actin cytoskeleton and especially on the membrane spikes, which were more decreased upon treatment with polyacrylate and even more upon treatment with the copper-polyacrylate complex.

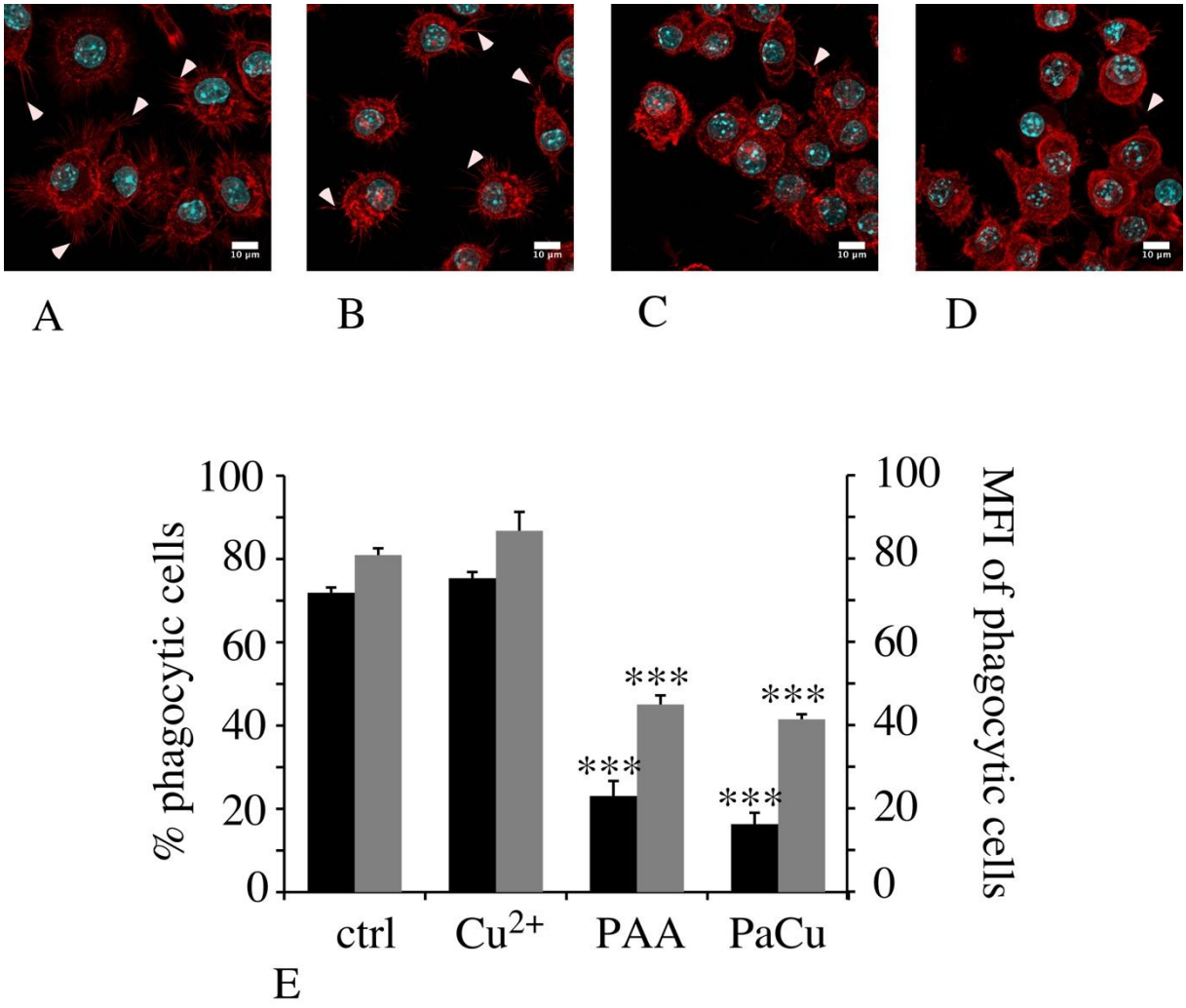

Figure 6 : Actin cytoskeleton and phagocytosis

In panels A-D, the actin cytoskeleton was visualized with fluorescent phalloidin and confocal microscopy. Only one confocal plane inside the cells is shown (going through the cell nucleus)
Examples of membrane spikes are indicated by white arrowheads
A : unexposed cells
B : cells exposed to 150 µM copper sulfate
C ; cells exposed to 0.25 mg/ml polyacrylate
D : cells exposed to 0.25 mg/ml polyacrylate + 150µM copper sulfate

In panel E, the phagocytic capacity was assessed by fluorescent latex beads internalization
black bars: proportion of positive cells in the viable cell population
grey bars : mean cellular fluorescence
Ctrl : unexposed cells
Cu^{2+} : cells exposed to 150 µM copper sulfate
PAA ; cells exposed to 0.25 mg/ml polyacrylate
PaCu : cells exposed to 0.25 mg/ml polyacrylate + 150µM copper sulfate

Symbols indicate the statistical significance (Student T- test): *: $p<0.05$; **:$p<0.01$; ***: $p<0.001$

Phagocytosis is one of the major functions of macrophages, and depends on the actomyosin system. We thus tested this function, as changes in lysosomes-associated proteins were also

observed. The results, on **Figure 6E**, indicated no effect of copper ion but an important and similar effect of polyacrylate and copper-polyacrylate complex, both in the proportion of phagocytic cells and in the phagocytic capacity of the phagocytic cells.
Combined with previous results obtained on copper ion and nanoparticles [38], these results clearly show that copper ion at subtoxic concentrations has no impact on phagocytosis. An impact is obtained only when the endosomal/lysosomal pathway is at play, either by a polymer binding to the scavenger receptor (polyacrylate here) or by nanoparticles [38]. These nanoparticles do not need to contain copper, as silica nanoparticles or carbon nanotubes also induce a decrease in the phagocytic activity [40,67,68]. The only case in which an effect of copper on phagocytosis without being macromolecular or particular is as a hydroxyquinoline complex [27]. In this case however, we do not know whether the hydroxyquinoline ionophore brings copper only in the cytosol or is also able to bring copper into the endosomes.
In the frame of this study, it is also worth noting that a fair proportion of the proteins that are selectively and significantly modulated by the copper-polyacrylate treatment (**Suppl. Table 5**) are cytoskeletal proteins, which correlates well with the massive alteration of the cytoskeleton observed upon treatment with the copper complex.
Taken at a higher level, cell shape and cytoskeleton involve a large number of proteins. This suggests that important changes in cell shape such as those observed in response to polyacrylate and copper-polyacrylate involve a large number of changes at the protein level or at the proteoform level, as many proteins involved in the cytoskeleton are controlled by phosphorylation (e.g. cofilin [69], Rho GDIs [70], arpc5[71], gelsolin [72] or Arp2 [73]). Consequently, many coordinated changes of maybe weak amplitude can be expected when cell shape changes. This may explain why such changes are strongly detected in the global proteomic data screening (i.e. hierarchical clustering) but not as easily by individual protein detection.

3.9. The inflammatory responses are altered in a complex way by copper and by polyacrylate

Although inflammatory responses did not appear in the pathway analysis, analysis of the proteomic data showed modulations of several proteins pointing at potential changes in the inflammatory responses upon exposure to copper and/or polyacrylate. For example, 2D gel-based proteomics highlighted modulations of nmrl1 (Q8K2T1), tollip (Q9QZ06), vps29 (Q9QZ88) and latexin (P70202). This prompted us to investigate the inflammatory responses with and without an additional stimulation by LPS. Responses without LPS stimulation point at the intrinsic effects of the treatments with copper and/or polyacrylate, while responses with LPS stimulation point at the interference of the treatments with the responses of macrophages to bacteria. The results, shown on **Figure 7,** indicate no effect of polyacrylate (except for LPS-induced NO and IL-6 production), but effects of copper. Rather surprisingly, basal production of NO and TNF followed opposite trends. NO production was induced upon treatment with copper ion and reduced upon treatment with polyacrylate±copper **(Figure 7A, black bars)**, while the opposite was observed for TNF **(Figure 7B)**. An increase in NO production was also observed upon treatment with the hydroxyquinoline-copper complex and with hydroxyquinoline alone [27] . This exemplifies another case in which the ancillary molecule used to modulate copper entry had an intrinsic effect, just as polyacrylate alone for phagocytosis. These results also showed that copper polyacrylate did not behave as other forms of copper for NO production.

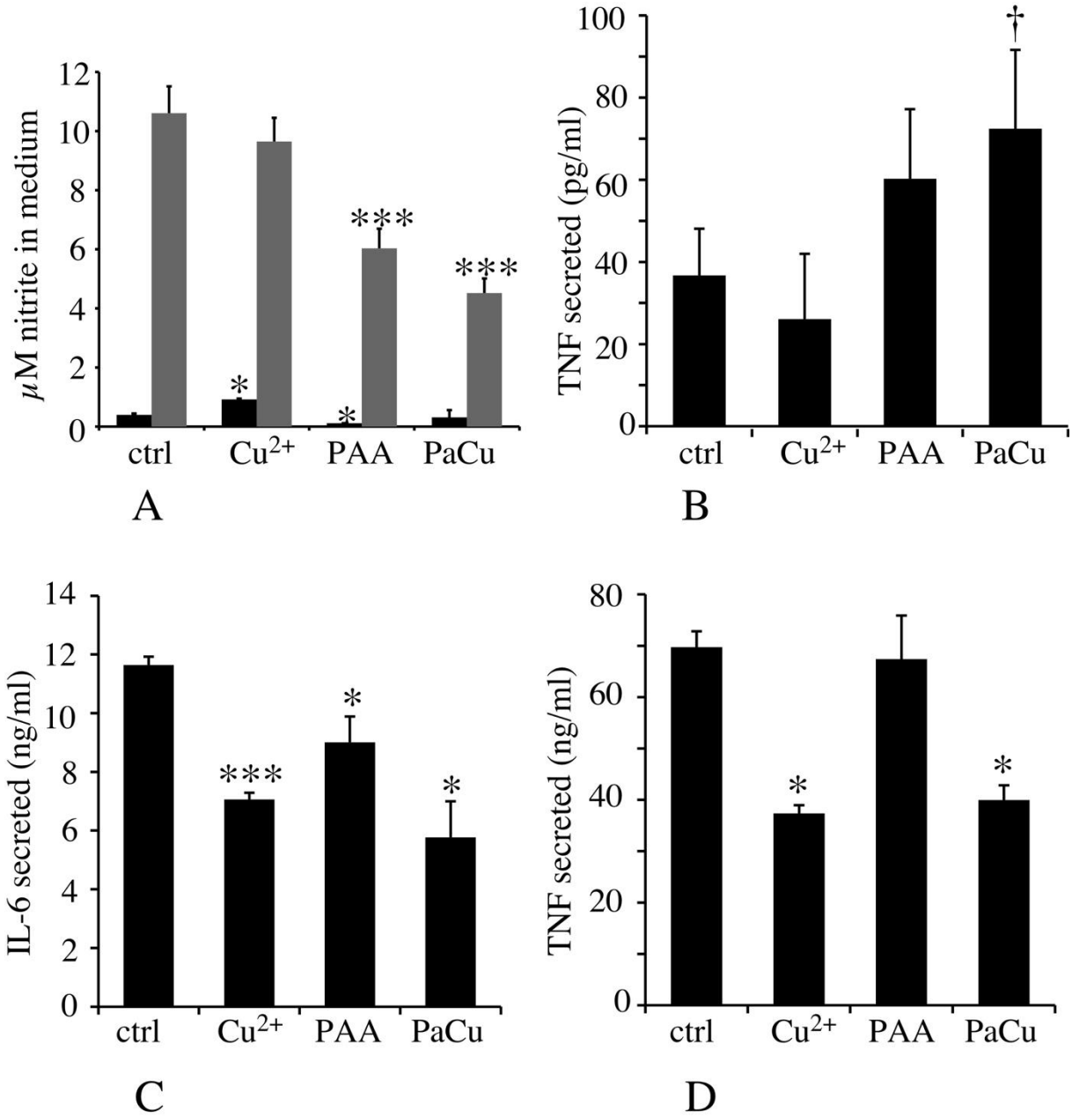

Figure 7 : inflammatory responses
The secretion of NO, Interleukin-6 and TNF alpha was measured in response to either copper alone, or to both copper and LPS.

Ctrl : unexposed cells
Cu^{2+} : cells exposed to 150 µM copper sulfate
PAA ; cells exposed to 0.25 mg/ml polyacrylate
PaCu : cells exposed to 0.25 mg/ml polyacrylate + 150µM copper sulfate

A : Production of nitric oxide
black bars : production after treatment for 24 hours with copper and/or polyacrylate
grey bars : production after treatment for 24 hours with copper and/or polyacrylate and stimulation with LPS for the last 18 hours of culture.

B: production of TNF in absence of LPS stimulation

C: production of interleukin-6 in the presence of LPS stimulation
(no interleukin-6 secretion was detected in the absence of LPS stimulation)

D : production of TNF in the presence of LPS stimulation

Symbols indicate the statistical significance (Student T- test): *: $p<0.05$; **:$p<0.01$; ***: $p<0.001$. † $p<0.05$ in the Mann-Whitney U-test

In the case of LPS-induced secretions, pre-treatment with copper ion or copper complex always induced a decrease in the production of pro-inflammatory mediators, whether NO (**Figure 7A, grey bars**) or interleukin 6 **(Figure 7C**) or TNF (**Figure 7D**). This decrease of NO production after LPS stimulation has been already observed on another macrophage cell line with copper ion, copper oxide nanoparticles [38] and hydroxyquinoline-copper complex [27]. Of note, polyacrylate alone also induced a decrease in the response to LPS, both for NO (**Figure 7A, grey bars**) and for interleukin 6 **(Figure 7C)**, but not for TNF (**Figure 7D**). Such decoupled responses for NO, interleukin 6 and TNF after LPS stimulation has been observed for silver and silica nanoparticles [56,57], which both enter macrophages using scavenger receptor [74,75], as polyacrylate [43].

4. Concluding remarks

Together with previous work carried out under slightly different conditions on the hydroxyquinoline-copper complex [27] or on copper nanoparticles [38], this work allows comparing the effects of copper ion under three different entry modes, i.e. as ion alone, hydroxyquinoline-copper complex and copper-polyacrylate complex. Some basic responses are shared by all entry modes, such as the decrease in the free glutathione concentration or the maintaining of the mitochondrial transmembrane potential, at least under sub-toxic conditions. Some differentiated responses of the macrophages are also shared by all forms of copper ion, such as the reduction in the LPS-induced NO production.
Conversely, different responses can be observed with different forms of copper. For example, a reduction in the phagocytic capacity is observed with both copper complexes but not with copper ion. Even more specifically, central metabolic enzyme activities (except enolase) are altered by the copper-polyacrylate complex but not with copper ion. These differential responses cannot be simply attributed to intracellular copper levels, as these are not significantly different between copper ion and copper-polyacrylate complex. Thus, subtle differences in the entry mode of copper or synergies with the polyacrylate carrier may explain these differences, although the molecular details underlying these differences are still unclear.

Authors contributions

JD, AT and SR performed the copper assay experiments. BD performed the phagocytosis, inflammatory response, confocal microscopy and mitochondrial potential experiments. VCF and TR performed the 2D gel experiments. TR performed the glutathione assay experiments. JB, HD, CC and SC performed and reviewed the mass spectrometry experiments. TR prepared the initial draft of the manuscript, which was reviewed and amended by all co-authors.

Conflicts of interests

The authors declare no conflict of interest

Acknowledgments

This work was funded by the CNRS and the University Grenoble-Alpes. This work used the platforms of the French Proteomic Infrastructure (ProFI) project (grant ANR-10-INBS-08-03) and of GRAL, a programme from the Chemistry Biology Health (CBH) Graduate School of University Grenoble Alpes (ANR-17-EURE-0003).

On a more scientific level, the authors would like to thank the curators of the Swissprot database for the quality of their functional annotations, which made the exploitation of the proteomic data much more fruitful and straightforward.

5. References

[1] P.C. Bull, D.W. Cox, Wilson disease and Menkes disease: new handles on heavy-metal transport, Trends Genet. 10 (1994) 246–52.

[2] B. Dixon, Pushing Bordeaux mixture, Lancet Infect Dis. 4 (2004) 594.

[3] J.C. Pimentel, A.P. Menezes, Liver granulomas containing copper in vineyard sprayer's lung. A new etiology of hepatic granulomatosis, Am Rev Respir Dis. 111 (1975) 189–95.

[4] K.G. Daniel, P. Gupta, R.H. Harbach, W.C. Guida, Q.P. Dou, Organic copper complexes as a new class of proteasome inhibitors and apoptosis inducers in human cancer cells, Biochemical Pharmacology. 67 (2004) 1139–1151.

[5] K.G. Daniel, D. Chen, S. Orlu, Q.C. Cui, F.R. Miller, Q.P. Dou, Clioquinol and pyrrolidine dithiocarbamate complex with copper to form proteasome inhibitors and apoptosis inducers in human breast cancer cells, Breast Cancer Research. 7 (2005) R897–R908.

[6] D. Chen, Q.P. Dou, New uses for old copper-binding drugs: converting the pro-angiogenic copper to a specific cancer cell death inducer, Expert Opinion on Therapeutic Targets. 12 (2008) 739–748.

[7] M.J. Petris, K. Smith, J. Lee, D.J. Thiele, Copper-stimulated endocytosis and degradation of the human copper transporter, hCtr1, J Biol Chem. 278 (2003) 9639–46.

[8] V. Oliveri, V. Lanza, D. Milardi, M. Viale, I. Maric, C. Sgarlata, G. Vecchio, Amino- and chloro-8-hydroxyquinolines and their copper complexes as proteasome inhibitors and antiproliferative agents, Metallomics. 9 (2017) 1439–1446.

[9] U. Jungwirth, C.R. Kowol, B.K. Keppler, C.G. Hartinger, W. Berger, P. Heffeter, Anticancer Activity of Metal Complexes: Involvement of Redox Processes, Antioxidants & Redox Signaling. 15 (2011) 1085–1127.

[10] J.L. Allensworth, M.K. Evans, F. Bertucci, A.J. Aldrich, R.A. Festa, P. Finetti, N.T. Ueno, R. Safi, D.P. McDonnell, D.J. Thiele, S. Van Laere, G.R. Devi, Disulfiram (DSF) acts as a copper ionophore to induce copper-dependent oxidative stress and mediate anti-tumor efficacy in inflammatory breast cancer, Mol Oncol. 9 (2015) 1155–68.

[11] M. Amici, K. Forti, C. Nobili, G. Lupidi, M. Angeletti, E. Fioretti, A.M. Eleuteri, Effect of neurotoxic metal ions on the proteolytic activities of the 20S proteasome from bovine brain, J Biol Inorg Chem. 7 (2002) 750–6.

[12] M.A. Cater, H.B. Pearson, K. Wolyniec, P. Klaver, M. Bilandzic, B.M. Paterson, A.I. Bush, P.O. Humbert, S. La Fontaine, P.S. Donnelly, Y. Haupt, Increasing Intracellular Bioavailable Copper Selectively Targets Prostate Cancer Cells, Acs Chemical Biology. 8 (2013) 1621–1631.

[13] E.E. Manasanch, R.Z. Orlowski, Proteasome inhibitors in cancer therapy, Nat Rev Clin Oncol. 14 (2017) 417–433.

[14] F.N. Akladios, S.D. Andrew, C.J. Parkinson, Selective induction of oxidative stress in cancer cells via synergistic combinations of agents targeting redox homeostasis, Bioorg Med Chem. 23 (2015) 3097–104.

[15] S. Chatterjee, P. Chakraborty, K. Banerjee, A. Sinha, A. Adhikary, T. Das, S.K. Choudhuri, Selective induction of apoptosis in various cancer cells irrespective of drug sensitivity through a copper chelate, copper N-(2 hydroxy acetophenone) glycinate: crucial involvement of glutathione, Biometals. 26 (2013) 517–34.

[16] D. Denoyer, H.B. Pearson, S.A. Clatworthy, Z.M. Smith, P.S. Francis, R.M. Llanos, I. Volitakis, W.A. Phillips, P.M. Meggyesy, S. Masaldan, M.A. Cater, Copper as a target for prostate cancer therapeutics: copper-ionophore pharmacology and altering systemic

copper distribution, Oncotarget. 7 (2016) 37064–37080.
[17] W. Zou, Immunosuppressive networks in the tumour environment and their therapeutic relevance, Nat Rev Cancer. 5 (2005) 263–74.
[18] S.L. Shiao, A.P. Ganesan, H.S. Rugo, L.M. Coussens, Immune microenvironments in solid tumors: new targets for therapy, Genes Dev. 25 (2011) 2559–72.
[19] E.V. Polishchuk, R.S. Polishchuk, The emerging role of lysosomes in copper homeostasis, Metallomics. 8 (2016) 853–62.
[20] H. Ohrvik, B. Logeman, G. Noguchi, I. Eriksson, L. Kjellen, D.J. Thiele, G. Pejler, Ctr2 Regulates Mast Cell Maturation by Affecting the Storage and Expression of Tryptase and Proteoglycans, J Immunol. 195 (2015) 3654–64.
[21] P.V. van den Berghe, D.E. Folmer, H.E. Malingre, E. van Beurden, A.E. Klomp, B. van de Sluis, M. Merkx, R. Berger, L.W. Klomp, Human copper transporter 2 is localized in late endosomes and lysosomes and facilitates cellular copper uptake, Biochem J. 407 (2007) 49–59.
[22] J. George, R. Singh, Z. Mahmood, Y. Shukla, Toxicoproteomics: New paradigms in toxicology research, Toxicology Mechanisms and Methods. 20 (2010) 415–423.
[23] T. Rabilloud, P. Lescuyer, Proteomics in mechanistic toxicology: history, concepts, achievements, caveats, and potential, Proteomics. 15 (2015) 1051–1074.
[24] S. Suman, S. Mishra, Y. Shukla, Toxicoproteomics in human health and disease: an update, Expert Rev Proteomics. 13 (2016) 1073–1089.
[25] G. Repetto, A. del Peso, J.L. Zurita, Neutral red uptake assay for the estimation of cell viability/cytotoxicity, Nat Protoc. 3 (2008) 1125–31.
[26] T. Rabilloud, Optimization of the cydex blue assay: A one-step colorimetric protein assay using cyclodextrins and compatible with detergents and reducers, PLoS One. 13 (2018) e0195755.
[27] B. Dalzon, J. Bons, H. Diemer, V. Collin-Faure, C. Marie-Desvergne, M. Dubosson, S. Cianferani, C. Carapito, T. Rabilloud, A Proteomic View of Cellular Responses to Anticancer Quinoline-Copper Complexes, Proteomes. 7 (2019) 26.
[28] J.A. Vizcaino, A. Csordas, N. Del-Toro, J.A. Dianes, J. Griss, I. Lavidas, G. Mayer, Y. Perez-Riverol, F. Reisinger, T. Ternent, Q.W. Xu, R. Wang, H. Hermjakob, 2016 update of the PRIDE database and its related tools, Nucleic Acids Res. 44 (2016) 11033.
[29] O. Hammer, D.A.T. Harper, Ryan P. D, Paleontological statistics software package for education and data analysis, Palaeontologia Electronica. 4 (2001) 9pp.
[30] K.M. Mayer, F.H. Arnold, A colorimetric assay to quantify dehydrogenase activity in crude cell lysates, J Biomol Screen. 7 (2002) 135–40.
[31] P.D. Simcox, E.E. Reid, D.T. Canvin, D.T. Dennis, Enzymes of the Glycolytic and Pentose Phosphate Pathways in Proplastids from the Developing Endosperm of *Ricinus communis* L, Plant Physiol. 59 (1977) 1128–32.
[32] P. Fossati, Phosphate determination by enzymatic colorimetric assay, Anal Biochem. 149 (1985) 62–5.
[33] V.E. Anderson, P.M. Weiss, W.W. Cleland, Reaction intermediate analogues for enolase, Biochemistry. 23 (1984) 2779–2786.
[34] C. Salerno, J. Ovádi, T. Keleti, P. Fasella, Kinetics of coupled reactions catalyzed by aspartate aminotransferase and glutamate dehydrogenase, Eur. J. Biochem. 121 (1982) 511–517.
[35] B. Mannervik, B. Gorna-Hall, T. Bartfai, The steady-state kinetics of glyoxalase I from porcine erythrocytes. Evidence for a random-pathway mechanism involving one- and two-substrate branches, Eur J Biochem. 37 (1973) 270–81.
[36] R.E. Manrow, R.P. Dottin, Demonstration, by renaturation in O'Farrell gels, of heterogeneity in Dictyostelium uridine diphosphoglucose pyrophosphorylase, Analytical

Biochemistry. 120 (1982) 181–188.
[37] G. Abel, J. Szollosi, J. Fachet, Phagocytosis of fluorescent latex microbeads by peritoneal macrophages in different strains of mice: a flow cytometric study, Eur J Immunogenet. 18 (1991) 239–45.
[38] S. Triboulet, C. Aude-Garcia, M. Carriere, H. Diemer, F. Proamer, A. Habert, M. Chevallet, V. Collin-Faure, J.M. Strub, D. Hanau, A. Van Dorsselaer, N. Herlin-Boime, T. Rabilloud, Molecular responses of mouse macrophages to copper and copper oxide nanoparticles inferred from proteomic analyses, Mol Cell Proteomics. 12 (2013) 3108–3122.
[39] C. Aude-Garcia, B. Dalzon, J.L. Ravanat, V. Collin-Faure, H. Diemer, J.M. Strub, S. Cianferani, A. Van Dorsselaer, M. Carriere, T. Rabilloud, A combined proteomic and targeted analysis unravels new toxic mechanisms for zinc oxide nanoparticles in macrophages, Journal of Proteomics. 134 (2016) 174–185.
[40] B. Dalzon, C. Aude-Garcia, V. Collin-Faure, H. Diemer, D. Béal, F. Dussert, D. Fenel, G. Schoehn, S. Cianférani, M. Carrière, T. Rabilloud, Differential proteomics highlights macrophage-specific responses to amorphous silica nanoparticles, Nanoscale. 9 (2017) 9641–9658.
[41] S.W. Perry, J.P. Norman, J. Barbieri, E.B. Brown, H.A. Gelbard, Mitochondrial membrane potential probes and the proton gradient: a practical usage guide, Biotechniques. 50 (2011) 98–115.
[42] M. Warholm, C. Guthenberg, C. von Bahr, B. Mannervik, Glutathione transferases from human liver, Methods Enzymol. 113 (1985) 499–504.
[43] M. Fujiwara, J.D. Baldeschwieler, R.H. Grubbs, Receptor-mediated endocytosis of poly(acrylic acid)-conjugated liposomes by macrophages, Biochim Biophys Acta. 1278 (1996) 59–67.
[44] J.H. Kaplan, E.B. Maryon, How Mammalian Cells Acquire Copper: An Essential but Potentially Toxic Metal, Biophys J. 110 (2016) 7–13.
[45] A. Espinoza, S. Le Blanc, M. Olivares, F. Pizarro, M. Ruz, M. Arredondo, Iron, copper, and zinc transport: inhibition of divalent metal transporter 1 (DMT1) and human copper transporter 1 (hCTR1) by shRNA, Biol Trace Elem Res. 146 (2012) 281–6.
[46] T. Sone, K. Yamaoka, Y. Minami, H. Tsunoo, Induction of metallothionein synthesis in Menkes' and normal lymphoblastoid cells is controlled by the level of intracellular copper, J Biol Chem. 262 (1987) 5878–5885.
[47] S.D. Smith, Y.M. She, E.A. Roberts, B. Sarkar, Using immobilized metal affinity chromatography, two-dimensional electrophoresis and mass spectrometry to identify hepatocellular proteins with copper-binding ability, J Proteome Res. 3 (2004) 834–40.
[48] C. Chen, Y. Song, K. Zhuang, L. Li, Y. Xia, Z. Shen, Proteomic Analysis of Copper-Binding Proteins in Excess Copper-Stressed Roots of Two Rice (*Oryza sativa* L.) Varieties with Different Cu Tolerances, PLoS One. 10 (2015) e0125367.
[49] M. Salim, B.A. Brown-Kipphut, M.D. Maines, Human Biliverdin Reductase Is Autophosphorylated, and Phosphorylation Is Required for Bilirubin Formation, Journal of Biological Chemistry. 276 (2001) 10929–10934.
[50] Y. Xiong, K.L. Guan, Mechanistic insights into the regulation of metabolic enzymes by acetylation, J Cell Biol. 198 (2012) 155–64.
[51] H. Weber, S. Engelmann, D. Becher, M. Hecker, Oxidative stress triggers thiol oxidation in the glyceraldehyde-3-phosphate dehydrogenase of Staphylococcus aureus, Mol. Microbiol. 52 (2004) 133–140. .
[52] P. Tarroux, Analysis of Protein-Patterns During Differentiation Using 2-D Electrophoresis and Computer Multidimensional Classification, Electrophoresis. 4 (1983) 63–70.

[53] P. Tarroux, P. Vincens, T. Rabilloud, Hermes - a 2nd Generation Approach to the Automatic-Analysis of Two-Dimensional Electrophoresis Gels .5. Data-Analysis, Electrophoresis. 8 (1987) 187–199.
[54] T. Pun, D.F. Hochstrasser, R.D. Appel, M. Funk, V. Villars-Augsburger, C. Pellegrini, Computerized classification of two-dimensional gel electrophoretograms by correspondence analysis and ascendant hierarchical clustering, Appl Theor Electrophor. 1 (1988) 3–9.
[55] B. Dalzon, A. Torres, H. Diemer, S. Ravanel, V. Collin-Faure, K. Pernet-Gallay, P.-H. Jouneau, J. Bourguignon, S. Cianf√©rani, M. Carri√®re, C. Aude-Garcia, T. Rabilloud, How reversible are the effects of silver nanoparticles on macrophages? A proteomic-instructed view, Environmental Science: Nano. 6 (2019) 3133–3157.
[56] B. Dalzon, C. Aude-Garcia, H. Diemer, J. Bons, C. Marie-Desvergne, J. Pérard, M. Dubosson, V. Collin-Faure, C. Carapito, S. Cianférani, M. Carrière, T. Rabilloud, The longer the worse: a combined proteomic and targeted study of the long-term *versus* short-term effects of silver nanoparticles on macrophages, Environ. Sci.: Nano. 7 (2020) 2032–2046.
[57] A. Torres, B. Dalzon, V. Collin-Faure, H. Diemer, D. Fenel, G. Schoehn, S. Cianférani, M. Carrière, T. Rabilloud, How Reversible Are the Effects of Fumed Silica on Macrophages? A Proteomics-Informed View, Nanomaterials (Basel). 10 (2020) 1939.
[58] D.W. Huang, B.T. Sherman, R.A. Lempicki, Bioinformatics enrichment tools: paths toward the comprehensive functional analysis of large gene lists, Nucleic Acids Res. 37 (2009) 1–13.
[59] T. Rabilloud, P. Lescuyer, The proteomic to biology inference, a frequently overlooked concern in the interpretation of proteomic data: a plea for functional validation, Proteomics. 14 (2014) 157–161. .
[60] K. Marcus, T. Rabilloud, How Do the Different Proteomic Strategies Cope with the Complexity of Biological Regulations in a Multi-Omic World? Critical Appraisal and Suggestions for Improvements, Proteomes. 8 (2020) 23.
[61] J. Bons, C. Macron, C. Aude-Garcia, S.A. Vaca-Jacome, M. Rompais, S. Cianferani, C. Carapito, T. Rabilloud, A Combined N-terminomics and Shotgun Proteomics Approach to Investigate the Responses of Human Cells to Rapamycin and Zinc at the Mitochondrial Level, Mol Cell Proteomics. 18 (2019) 1085–1095.
[62] J.V. Olsen, M. Vermeulen, A. Santamaria, C. Kumar, M.L. Miller, L.J. Jensen, F. Gnad, J. Cox, T.S. Jensen, E.A. Nigg, S. Brunak, M. Mann, Quantitative phosphoproteomics reveals widespread full phosphorylation site occupancy during mitosis, Sci Signal. 3 (2010) ra3.
[63] J. Fang, S. Qiao, K. Wang, R. Li, L. Wang, H. Li, G. Zhang, Quantitative Proteomic Analysis of Global Protein Acetylation in PRRSV-Infected Pulmonary Alveolar Macrophages, Proteomics. (2020) e2000019.
[64] Z.N. Baker, P.A. Cobine, S.C. Leary, The mitochondrion: a central architect of copper homeostasis, Metallomics. 9 (2017) 1501–1512.
[65] Y. Chen, H.G. Shertzer, S.N. Schneider, D.W. Nebert, T.P. Dalton, Glutamate cysteine ligase catalysis: dependence on ATP and modifier subunit for regulation of tissue glutathione levels, J Biol Chem. 280 (2005) 33766–74.
[66] C. D'Anna, D. Cigna, C. Di Sano, S. Di Vincenzo, P. Dino, M. Ferraro, L. Bini, L. Bianchi, F. Di Gaudio, M. Gjomarkaj, E. Pace, Exposure to cigarette smoke extract and lipopolysaccharide modifies cytoskeleton organization in bronchial epithelial cells, Exp Lung Res. 43 (2017) 347–358.
[67] R. Wang, M. Lee, K. Kinghorn, T. Hughes, I. Chuckaree, R. Lohray, E. Chow, P. Pantano, R. Draper, Quantitation of cell-associated carbon nanotubes: selective binding and

accumulation of carboxylated carbon nanotubes by macrophages, Nanotoxicology. 12 (2018) 677–698.
[68] A. Torres, B. Dalzon, V. Collin-Faure, T. Rabilloud, Repeated vs. Acute Exposure of RAW264.7 Mouse Macrophages to Silica Nanoparticles: A Bioaccumulation and Functional Change Study, Nanomaterials. 10 (2020) 215.
[69] N. Yang, O. Higuchi, K. Ohashi, K. Nagata, A. Wada, K. Kangawa, E. Nishida, K. Mizuno, Cofilin phosphorylation by LIM-kinase 1 and its role in Rac-mediated actin reorganization, Nature. 393 (1998) 809–812.
[70] C. DerMardirossian, G. Rocklin, J.-Y. Seo, G.M. Bokoch, Phosphorylation of RhoGDI by Src regulates Rho GTPase binding and cytosol-membrane cycling, Mol. Biol. Cell. 17 (2006) 4760–4768.
[71] R. Silverman-Gavrila, L. Silverman-Gavrila, G. Hou, M. Zhang, M. Charlton, M.P. Bendeck, Rear polarization of the microtubule-organizing center in neointimal smooth muscle cells depends on PKCα, ARPC5, and RHAMM, Am. J. Pathol. 178 (2011) 895–910.
[72] P. Singaravelu, W.L. Lee, S. Wee, U. Ghoshdastider, K. Ding, J. Gunaratne, J.M. Grimes, K. Swaminathan, R.C. Robinson, Yersinia effector protein (YopO)-mediated phosphorylation of host gelsolin causes calcium-independent activation leading to disruption of actin dynamics, J. Biol. Chem. 292 (2017) 8092–8100.
[73] L.L. LeClaire, M. Baumgartner, J.H. Iwasa, R.D. Mullins, D.L. Barber, Phosphorylation of the Arp2/3 complex is necessary to nucleate actin filaments, J. Cell Biol. 182 (2008) 647–654.
[74] J.H. Shannahan, R. Podila, A.A. Aldossari, H. Emerson, B.A. Powell, P.C. Ke, A.M. Rao, J.M. Brown, Formation of a protein corona on silver nanoparticles mediates cellular toxicity via scavenger receptors, Toxicol Sci. 143 (2015) 136–146.
[75] G.A. Orr, W.B. Chrisler, K.J. Cassens, R. Tan, B.J. Tarasevich, L.M. Markillie, R.C. Zangar, B.D. Thrall, Cellular recognition and trafficking of amorphous silica nanoparticles by macrophage scavenger receptor A, Nanotoxicology. 5 (2011) 296–311